Journal of Computational Physics 229 (2010) 6574–6584

Contents lists available at ScienceDirect

Journal of Computational Physics

journal homepage: www.elsevier.com/locate/jcp

Diffuse-interface approach to predicting morphologies of critical nucleus and equilibrium structure for cubic to tetragonal transformations

Lei Zhang [a,*], Long-Qing Chen [b], Qiang Du [b,c]

[a] Department of Mathematics, University of California, Irvine, CA 92697, USA
[b] Department of Materials Science and Engineering, Pennsylvania State University, PA 16802, USA
[c] Department of Mathematics, Pennsylvania State University, PA 16802, USA

ARTICLE INFO

Article history:
Received 12 December 2009
Received in revised form 11 May 2010
Accepted 17 May 2010
Available online 23 May 2010

Keywords:
Phase-field
Diffuse-interface
Nucleation
Critical nucleus
Constrained string method
Elasticity
Cubic to tetragonal transformation

ABSTRACT

A cubic to tetragonal transformation leads to simultaneous nucleation and growth of several orientation variants. The size and morphology of a critical nucleus, comprising of one or more variants, are determined by the competition among bulk thermodynamic driving force, elastic strain energy, and interfacial energy. In this work, a diffuse-interface model is developed to predict both the critical nucleus morphology of a single variant tetragonal precipitate described by a conserved field and the critical morphology of a two-variant nucleus and equilibrium multivariant twinning microstructure resulted from a structural transformation described by non-conserved fields. A constrained string method was employed to compute the probable minimum energy paths and the microstructures along each path. Numerical experiments indicate that our approach works effectively for predicting the critical nucleus morphology both the precipitation processes and structural transformations.

1. Introduction

Nucleation in solid-state phase transformations is generally believed to be one of the most difficult processes to model. It takes place when a material becomes metastable with respect to its transformation to a new crystal structure. During a natural precipitation process in a supersaturated solid or liquid solution, e.g. during isothermal annealing of a quenched homogeneous alloy within a two-phase-field of a phase diagram, the majority of precipitation reactions in solids occur through a nucleation-and-growth mechanism followed by particle coarsening. There are two thermodynamically well-defined morphologies: the morphology of a critical nucleus and the equilibrium morphology of a precipitate particle. Predicting precipitate particle morphology in solids becomes a main challenge because of the presence of both interfacial energy anisotropy and anisotropic elastic interactions. Moreover, since the actual nucleation process is a rare event and the critical nucleus only exists transiently, it is of great interest for developing effective methods that can be used to study the morphological relation between the critical nucleus and the equilibrium precipitation.

The diffuse-interface description, or the nonclassical nucleation theory, is based on the gradient thermodynamics of nonuniform systems and provides a general framework of treating nucleation. Rather than assuming a particular geometry for a critical nucleus which is determined by a competition between a bulk free energy decrease which is proportional to volume and an interfacial energy increase which is proportional to interfacial area, a critical nucleus is defined as the composition or order parameter fluctuation having the minimum free energy increase among all fluctuations which lead to nucleation,

* Corresponding author. Tel.: +1 949 824 3217.
E-mail addresses: zhang14@uci.edu (L. Zhang), lqc3@psu.edu (L.-Q. Chen), qdu@math.psu.edu (Q. Du).

0021-9991/$ - see front matter © 2010 Elsevier Inc. All rights reserved.
doi:10.1016/j.jcp.2010.05.013

i.e., the saddle point configuration along the minimum energy path (MEP) between the metastable initial phase represented by a local minimum in the free energy landscape and the equilibrium phase represented by the global minimum. Therefore, nucleation of new phase particle requires overcoming a minimum thermodynamic barrier. The magnitude of the nucleation barrier, and thus the nucleation rate, or the resulted new phase particle density, is strongly dependent on the morphology of critical nucleus. On the other hand, following nucleation-and-growth, the morphology and volume fraction of new phase particle during coarsening are generally close to equilibrium. The particle morphology and volume fraction during coarsening together with the particle density predicted from nucleation provide the essential information that is needed for predicting the strength of a solid in mechanistic models.

Early studies of equilibrium shapes in solids often use both sharp- and diffuse-interface approaches [1–4,14,15]. Recent attempts have also been made to predict the morphology of a critical nucleus in solids by taking into account both interfacial energy anisotropy and anisotropic elastic interactions [16–18,20–23]. For example, we showed that one can predict the morphology of a critical nucleus in a system going through a phase transition [20,21] using a combination of the diffuse-interface (phase-field) description and the minimax algorithm based on the mountain pass theorem [12,22]. Diffuse-interface critical nuclei have also been incorporated in the dynamic phase-field simulation through the explicit nucleation algorithm in [28]. Recently, in [23], a new approach is developed to simultaneously predict the morphology of a critical nucleus as well as the equilibrium morphology of a precipitate within the same diffuse-interface model described by a single phase-field function. In this paper, we consider the more complex nucleation in cubic to tetragonal transformations which leads to the various crystallographic orientation variants (structure domains). Computationally, our approach is based on the calculation of MEPs with the unconstrained and constrained string methods which we describe in Section 2. We also compare such an approach with the corresponding modification to the Nudged Elastic Band method. The main results of the paper are given in Section 3. There, we first discuss the diffuse-interface model corresponding to the cubic to tetragonal transformations, with either a single order parameter or a pair of phase-field functions. We then present the algorithm for computing both the critical nucleus and the equilibrium microstructure simultaneously by combining the diffuse-interface model with the constrained string method. Results of several numerical examples in the single order parameter case are provided. An example on the extension to the two-variant nucleation case is also shown. These examples demonstrate the great potential in enlarging the applicability of our method to the complex cubic to tetragonal nucleation. Final conclusions are given in Section 4.

2. Method

2.1. String method

In the diffuse-interface theory of Cahn–Hilliard, phase-field variables such as order parameters or compositions are utilized to describe the structural transitions or concentration distributions in solids. Based on the transition state theory, the point (state) with the highest energy along the minimum energy path (MEP), a saddle point in general, defines the critical nucleus configuration, and the critical nucleation energy that determines the rate of a nucleation reaction. By the calculus of variations of the total free energy functional subject to external constraints, we know that the saddle points are unstable stationary points and they cannot be computed via the conventional total free energy minimization approaches.

In the last decade or so, several numerical methods have been developed for computing the saddle points and MEPs, including the Nudged Elastic Band (NEB) method [5,6] and more recently the string method and its various improvements [7,8]. The relevant saddle point can be identified with the highest energy point on the MEP [12]. In practical applications, the computation of MEPs and/or saddle points may be subject to one or more constraints. In [19,23], we adopted the idea of string method and the method of Lagrange multipliers to develop a constrained string method for finding the MEPs and saddle points subject to general constraints. Similar extensions to incorporate constraints can also be made to the NEB method which is to be shown later. We note that an interesting and yet different application of the string method to the study of nucleation in a constrained setting has been presented recently in [11] which also contained a comprehensive discussion on a variety of implementation strategies.

The original string methods [7,8] proceed by evolving a string, i.e., a smooth curve with intrinsic parametrization, to the MEP between two metastable/stable regions in the configuration space. Specifically, let $\varphi(\alpha,t)$ denote the instantaneous position (representing the composition/order parameter profile in our case) of the string with α being a suitable parametrization. For an energy $E = E(\varphi)$, the *canonical string dynamics* is

$$\begin{cases} \varphi_t = -\nabla E(\varphi)^{\perp} + \bar{\lambda}\hat{\tau}, \\ (|\varphi_\alpha|)_\alpha = 0, \end{cases} \tag{1}$$

where $\bar{\lambda}$ is a Lagrange multiplier for enforcing the particular parametrization of the string and $\hat{\tau}$ is the unit tangent of the curve φ.

For the numerical implementation, it was proposed in [8] to use the *simplified string method* based on a time-splitting scheme. The evolution of the string is based on first taking a gradient descent direction via the dynamic equation

$$\varphi_t = -\nabla E(\varphi),$$

then followed by a projection step that maps φ back to a configuration satisfying the specified parametrization. In practice, a commonly used parametrization for a string discretized by a finite number of line segments is to enforce an equal segment length condition through an interpolation procedure [8]. For recent applications of the string methods, we refer to [9–11,23].

2.2. Constrained string method

In search for MEPs, there may be additional physical constraints present on the feasible states. Without loss of generality, we denote

$$g(\varphi) = 0 \tag{2}$$

as a general constraint which may represent, for example, the constant concentration constraint, constant surface area constraint or any other constraints that may arise in applications.

By adopting the idea of string method and the method of Lagrange multipliers, we developed a constrained string method for finding the MEPs and saddle points subject to general constraints in [19,23]. The constrained string dynamics is given by

$$\begin{cases} \varphi_t = -\nabla E(\varphi)^{\perp} + \lambda^T \nabla g(\varphi) + \bar{\lambda}\hat{\tau}, \\ \nabla g \otimes \nabla g \lambda = \nabla g(\varphi) \nabla E^{\perp}, \\ (|\varphi_\alpha|)_\alpha = 0, \end{cases} \tag{3}$$

where, as in the improved string method, $\bar{\lambda}$ is the Lagrange multiplier determined by the parametrization, and the new parameter λ is the Lagrange multiplier associated with the constraint (2) with its dimension matches with that of the constraint function g. Here, the symbol $\otimes$ denotes the tensor product with entries of $\nabla g \otimes \nabla g \lambda$ given by $(\nabla g_i \cdot \nabla g_j)$ for g with components $\{g_i\}$. If g has a single component, then $\nabla g \otimes \nabla g = |\nabla g|^2$.

We notice that in the second equation of (3), λ is independent of the choice of parametrization $\bar{\lambda}$ [19]. Thus, in the numerical computation, the constrained string method can be efficiently implemented by adopting the simplified string method and using a time-splitting scheme.

Indeed, the constrained string method allows several equivalent formulations such as the penalty or Lagrange multiplier methods. Yet, some formulations are more natural and robust than others and require less parameter tuning. One particularly effective approach is based on the augmented Lagrange multiplier approach [13], which can be utilized to modify the total energy by

$$E_{ALM}(\varphi) = E(\varphi) + \lambda^T g(\varphi) + \frac{M}{2} g(\varphi)^2, \tag{4}$$

where M is a finite penalty constant.

The augmented Lagrangian method is then implemented via the following iterations [23]:

Step 1: Assume λ_j and φ_j are known, we apply the simplified string method to solve the dynamical equation:

$$(\varphi_j)_t = -\nabla E(\varphi_j) - \lambda_j^T \nabla g(\varphi_j) - M g(\varphi_j) \nabla g(\varphi_j).$$

Step 2: Once the solution of φ_j is obtained, we update

$$\lambda_{j+1} = \lambda_j + M g(\varphi_j) \nabla g(\varphi_j).$$

Then go back to Step 1 and iterate until convergence.

At the end of iteration, the constrained MEP is found with Eq. (2) satisfied along the string, and the limit of λ_j gives the corresponding Lagrange multiplier. Adopting this formulation, the implementation of the constrained string method is straightforward and it assures the satisfaction of the constraint without requiring M to be exceedingly large, thus reducing the stiffness of the dynamic system. For other implementation issues and applications of the constrained string method, we refer to [19,11,23]. Let us point out that the constrained string method with the augmented Lagrange multiplier formulation can also be derived for very general energies and constrained manifolds and thus have many potential applications.

2.3. Comparison with the NEB method

The NEB method [5,6] is another popular method for finding the MEP between the given initial and final states of a transition. A recent application of the NEB method is to use the free-end NEB algorithm in the computation critical nucleus in solid-state transformation [18]. Similar as the string method, NEB method is also a chain-of-states method. The discrete representation of a string is created and connected together with springs, then an optimization algorithm is applied to relax the string down towards the MEP.

With a continuum description, the NEB dynamics can be considered as the following evolution,

$$\varphi_t = -\nabla E(\varphi)^{\perp} + \kappa(\varphi_{\alpha\alpha}, \hat{\tau})\hat{\tau}, \tag{5}$$

where κ is the spring constant. While the string method and the NEB method are closely related, a key difference between them is in the use of different second terms on the right hand side of (1) and (5), which are aimed at preventing the images along the path from collapsing onto the local minima at the ends. In the string method, a particular parametrization is enforced, while in the NEB method, some artificial spring force is added along the path.

Naturally, one can also implement the NEB method in the constrained setting, much like what has been done for the string methods. Given a general constraint $g(\varphi) = 0$, the constrained NEB method is then

$$\begin{cases} \varphi_t = -\nabla E(\varphi)^{\perp} + \lambda^T \nabla g(\varphi) + \kappa(\varphi_{\alpha\alpha}, \hat{\tau})\hat{\tau}, \\ \nabla g \otimes \nabla g \lambda = \nabla g(\varphi) \nabla E^{\perp}, \end{cases} \tag{6}$$

where the parameter λ is the Lagrange multiplier.

Comparing (6) with (3), we notice that the second equations in (6) and (3) are the same. We thus see that the Lagrange multiplier λ is independent of the choice of the spring force in the constrained NEB method. This also provides much freedom in the design of the efficient algorithms.

2.4. Improvement of the saddle point calculation

The simplest case of parametrization for the string method is to enforce the equal arc-length on the string [8]. Given the values $\{\varphi_i\}$ on a possibly nonuniform mesh $\{\alpha_i\}$, the equal arc-length parametrization is done by interpolating these values onto a uniform mesh with the same number of points:

(1) Compute the arc-length by the current images,

$$s_0 = 0, \quad s_i = s_{i-1} + |\varphi_i - \varphi_{i-1}|, \quad i = 1, 2, \ldots, N.$$

The mesh $\{\alpha_i'\}$ is then obtained by normalizing $\{s_i\}$, i.e., $\alpha_i' = s_i/s_N$.

(2) Apply the linear/cubic interpolation to get the new images φ_i^{n+1} at the uniform grid points $\alpha_i = i/N$.

In some applications, a more accurate determination of the saddle point can be more important than computing the whole MEP precisely. It is suggested that [8], instead of the equal arc-length parametrization, a simple energy-weighted arc-length parametrization could be used in the string method, in order to have finer resolution around the saddle point, thus giving a better estimate of the energy barrier. This technique can be naturally extended to the constrained string method since the Lagrange multiplier for the extra constraint is independent of the parametrization. Thus, we can substitute the equal arc-length s_i by the weighted arc-length s_i^w by

$$s_0^w = 0, \quad s_i^w = s_{i-1}^w + W_i|\varphi_i - \varphi_{i-1}|, \quad i = 1, 2, \ldots, N,$$

where the weight function W is some positive and increasing function depending on the $E(\varphi_i)$. Examples of such a weight function include a polynomial type weight $W_i = (E(\varphi_i) - m + 1)^k$ with degree k, and an exponential type weight $W_i = \exp(E(\varphi_i) - m)$, where $m = \min_{1 \leqslant i \leqslant N}\{E(\varphi_i)\}$.

3. Application to cubic to tetragonal nucleation

We now describe the diffuse-interface model that can be used, in combination withe above discussed algorithms for MEP computations, to study the cubic to tetragonal nucleation in solid-state transformations.

3.1. Single composition profile in a conserved field

Following [26], we use the conserved field c to describe the concentration distribution in a binary solid. The total free energy, E_{total}, arising from the compositional fluctuation in an initially homogeneous state with c_0, is given by

$$E_{total}(c) = \int_{\Omega} \left(\frac{1}{2}|A\nabla c|^2 + \delta f(c) \right) d\mathbf{x} + \beta E_e(c). \tag{7}$$

For simplicity, we take the computational domain to be $\Omega = (-1, 1)^d$ with d being the space dimension. The gradient energy coefficient A is a constant diagonal tensor in Ω for isotropic interfacial energy, while for anisotropic interfacial energy, it can be made to be either directionally dependent or dependent on the derivatives of c.

The local free energy density change $\delta f(c)$ arising from a compositional fluctuation around the homogeneous state with composition c_0 is given by

$$\delta f(c) = \frac{1}{4\kappa}(c^2 - 1)^2 - \frac{1}{4\kappa}(c_0^2 - 1)^2 - \frac{1}{\kappa}(c - c_0)(c_0^3 - c_0),$$

where κ is a coefficient of energy density. The plots of $\delta f = \delta f(c)$ are given in Fig. 1 for different values of the average composition c_0 at $\kappa = 0.03$ with c_s being the spinodal composition given by $-\sqrt{3}/3$.

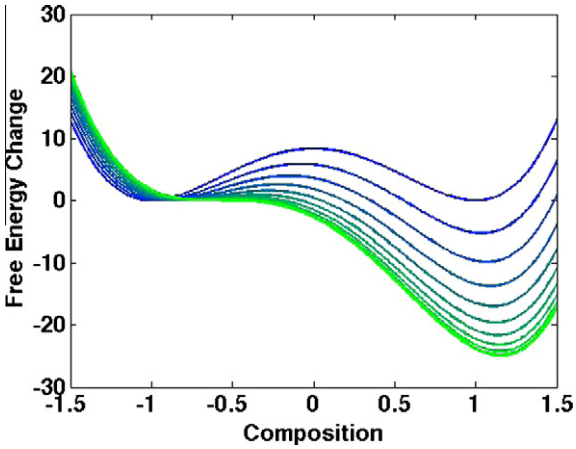

Fig. 1. Free energy change for c_0 from -1 (blue curve) to c_s (green curve) (For interpretation of the references in colour in this figure legend, the reader is referred to the web version of this article.).

The cubic to tetragonal crystal lattice rearrangement may be realized by a homogeneous strain of three different types leading to different orientations of the tetragonal axes, along the [100], [010] and [001] parent phase directions, respectively. These types of strain are described respectively by the matrices

$$\begin{pmatrix} \epsilon_{11}^0 & 0 & 0 \\ 0 & \epsilon_{11}^0 & 0 \\ 0 & 0 & \epsilon_{33}^0 \end{pmatrix}, \quad \begin{pmatrix} \epsilon_{11}^0 & 0 & 0 \\ 0 & \epsilon_{33}^0 & 0 \\ 0 & 0 & \epsilon_{11}^0 \end{pmatrix}, \quad \begin{pmatrix} \epsilon_{33}^0 & 0 & 0 \\ 0 & \epsilon_{11}^0 & 0 \\ 0 & 0 & \epsilon_{11}^0 \end{pmatrix}.$$

We assume that the elastic modulus is anisotropic but homogeneous so we may employ the microscopic elasticity theory of Khachaturyan [27]. For a cubic crystal, the elastic energy formula is written as

$$E_{elastic} = \frac{1}{2(2\pi)^d} \int_{\hat{\Omega}} d\mathbf{k} B(\mathbf{n}) |\hat{\eta}(\mathbf{k}) - \hat{\eta}_0(\mathbf{k})|^2. \tag{8}$$

Here, $\hat{\eta}(\mathbf{k})$ is the Fourier transform of $\eta(\mathbf{x})$, and the integration in (8) is over the reciprocal space $\hat{\Omega}$ of the reciprocal lattice vector $\mathbf{k}$, $\mathbf{n} = \mathbf{k}/|\mathbf{k}| = (n_1, n_2, n_3)$ is the normalized unit vector and in three dimensions, and the term $B(\mathbf{n})$ is given by

$$B(\mathbf{n}) = C_{ijkl}\epsilon_{ij}^0\epsilon_{kl}^0 - n_i\sigma_{ij}^0\Omega_{jl}(\mathbf{n})\sigma_{lm}^0 n_m,$$

where C_{ijkl} is the elastic modulus tensor, ϵ_{ij}^0 is the stress-free strain, σ_{ij}^0 is the elastic stress and Ω_{ij} is the inverse to the tensor $\Omega_{ij}^{-1}(\mathbf{n}) = C_{iklj}n_k n_l$.

For a cubic material with its three independent elastic constants c_{11}, c_{12} and c_{44} in Voigt's notation, the stress-free strain for cubic to tetragonal transition is given by the tensor

$$\epsilon_{ij}^0 = \begin{pmatrix} \epsilon_{11}^0 & 0 & 0 \\ 0 & \epsilon_{11}^0 & 0 \\ 0 & 0 & \epsilon_{33}^0 \end{pmatrix}.$$

We can then simplify $B(\mathbf{n})$ to get

$$B(\mathbf{n}) = \overline{B} - \frac{(\sigma_{33}^0)^2}{c_{11}} \Psi(\mathbf{n}), \tag{9}$$

where

$$\Psi(\mathbf{n}) = [\alpha_1^2 + An_3^2(1-n_3^2) - (\alpha_1^2 - 1)n_3^4 + \xi B n_1^2 n_2^2 n_3^2 + 2\xi\alpha_1^2 n_1^2 n_2^2] \times \left[1 + \xi\frac{c_{11}+c_{12}}{c_{11}}(n_1^2n_2^2 + n_1^2n_3^2 + n_2^2n_3^2) + \frac{c_{11}+2c_{12}+c_{44}}{c_{11}}\xi^2 n_1^2 n_2^2 n_3^2\right]^{-1}$$

and

$$\xi = \frac{c_{11} - c_{12} - 2c_{44}}{c_{44}}, \quad \alpha_1 = \frac{\sigma^0_{11}}{\sigma^0_{33}} = \frac{(c_{11} + c_{12})t_1 + c_{12}}{2c_{12}t_1 + c_{11}}, \quad t_1 = \frac{\epsilon^0_{11}}{\epsilon^0_{33}},$$

$$A = \frac{c_{11}}{c_{44}} + \alpha_1^2\left(\frac{c_{11}}{c_{44}} - 2\right) - 2\alpha_1\left(\frac{c_{12}}{c_{44}} + 1\right),$$

$$B = \frac{c_{11} + c_{12}}{c_{44}} + 2\alpha_1^2\frac{c_{11} - c_{44}}{c_{44}} - 4\alpha_1\frac{c_{12} + c_{44}}{c_{44}},$$

$$\sigma^0_{ij} = \lambda_{ijkl}\epsilon^0_{kl} = \begin{pmatrix} \sigma^0_{11} & 0 & 0 \\ 0 & \sigma^0_{11} & 0 \\ 0 & 0 & \sigma^0_{33} \end{pmatrix},$$

$$\sigma^0_{11} = (c_{11} + c_{12})\epsilon^0_{11} + c_{12}\epsilon^0_{33}, \quad \sigma^0_{33} = 2c_{12}\epsilon^0_{11} + c_{11}\epsilon^0_{33},$$

$$\overline{B} = \lambda_{ijkl}\epsilon^0_{ij}\epsilon^0_{kl} = 2\epsilon^0_{11}\sigma^0_{11} + \epsilon^0_{33}\sigma^0_{33}.$$

Rather than varying the magnitude of lattice mismatch and elastic constants, a factor β is introduced to study the effect of the relative elastic energy contribution to the chemical driving force on the critical nucleus morphology and equilibrium particle morphology. A periodic boundary condition is used for the composition profile c. The period is sufficiently large in comparison with the size of the nucleus and particle to minimize boundary effects. Meanwhile to provide high resolution to the states on the discretized string representing the composition profiles in the computational domain. We use the Fourier spectral method for the spatial discretization which has been both numerically demonstrated and theoretically analyzed to have superior accuracy than other low order schemes [25]. Due to the use of the first order splitting in the time integration, the gradient descent step is simply implemented by the semi-implicit time marching [24].

For a conserved field, its profile $c = c(x)$ is subject to the constraint

$$\int_\Omega (c(x) - c_0)dx = 0. \tag{10}$$

Using the model and the algorithm described above, both the critical nucleus and equilibrium particle with a conserved composition can be determined. As an illustration, we focus on the two-dimensional example of a cubic to tetragonal transformation within the homogeneous modulus approximation. The 2D formulation of the elastic energy can be derived in a similar manner as that in (8). The computational set-up and the parameters used are as follows. The initial state has a uniform composition with $c(x) = c_0$ in Ω. Then, for the MEP computation, one end of the string is fixed to be the initial state, and the other end of the string allows to move but it is taken generally within the energy well of the ground state or equilibrium solution. The point with the highest energy on the MEP is identified as the profile corresponding to a critical nucleus. The string is discretized by $m = 30$ points and the spatial simulation grid is maintained as 256×256. Numerical verification was conducted to ensure that the numerical results enjoy sufficient resolution. Since the critical nucleus is relatively small in comparison to the computational domain, the plots of critical nuclei are magnified by a factor of 2 in order to get a better view. For the next series of simulations, we take the average composition $c_0 = -0.86$, and parameters $A_1 = A_2 = 1.56 \times 10^{-4}$, $\kappa = 1.5$ and $c_{11} = 250$, $c_{12} = 150$, $c_{44} = 200$.

In Fig. 2, we plot the critical nucleus (left) and equilibrium solution (right) in the presence of the long-range elastic interactions and with $\beta = 1$, $\epsilon^0_{11} = 0.01$ and $\epsilon^0_{33} = 0.03$. The result shows that both the critical nucleus and the equilibrium particle display a plate-like shape due to the strong anisotropic elasticity, and we find that the composition value at the center of a critical nucleus (0.9278) is smaller than the composition of the equilibrium particle (0.9880). In Fig. 3, we show the energy plot along the MEP to demonstrate how the energy changes from the initial state (the left-end point) to the final equilibrium state (the right-end point) by passing the critical nucleus (the point with the highest energy). Moreover, since the competition among the interfacial energy, bulk energy, and elastic energy determines the characteristic of the nucleation process, we also plot three energies along the MEP in Fig. 3 with a zoomed-in insert showing the values of these energies around the saddle point.

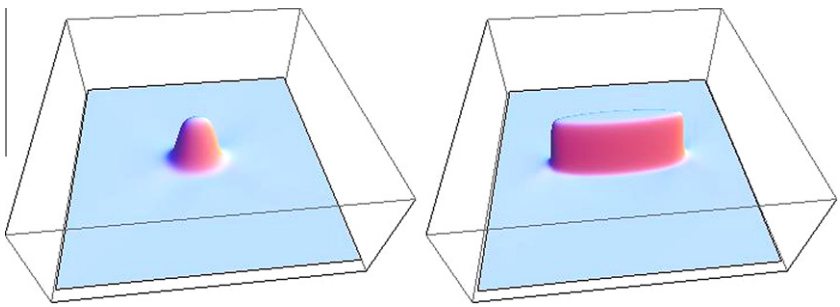

Fig. 2. Critical nucleus and equilibrium particle.

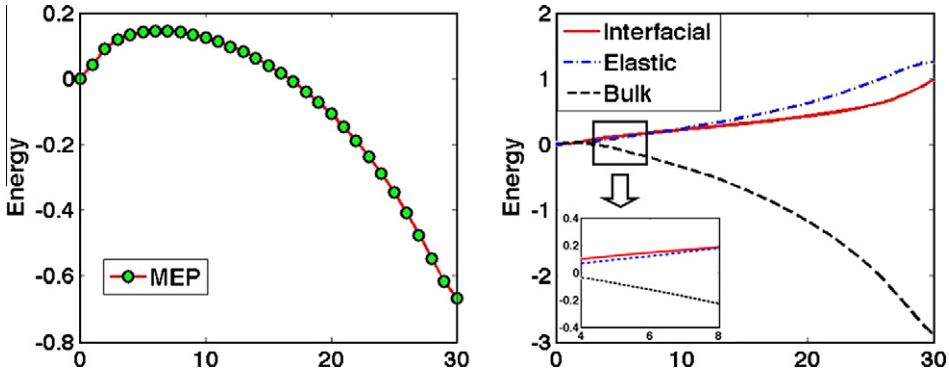

Fig. 3. MEP and plots of interfacial, elastic, and bulk energy.

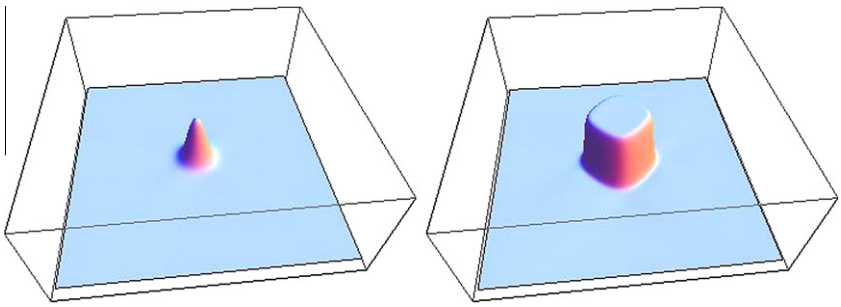

Fig. 4. Critical nucleus and equilibrium precipitate for $\beta = 1$.

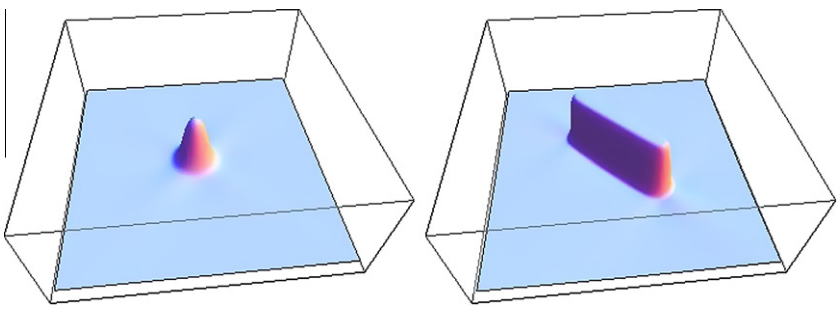

Fig. 5. Critical nucleus and equilibrium precipitate for $\beta = 2$.

In Fig. 4, we change the stress-free strain to $\epsilon^0_{11} = 0.02,\ \epsilon^0_{33} = -0.02$ and plot both the critical nucleus and the equilibrium at $\beta = 1$. For such a relatively small elastic energy contribution, both the critical nucleus and the equilibrium particle display a cubic symmetry. The shape of the critical nucleus is nearly circular while the equilibrium particle displays a diamond shape.

To examine the effect of elastic energy contributions, we fix the chemical driving force and increase β to compute the MEPs. In Fig. 5, we choose $\beta = 2$ and compute both the critical nucleus and the equilibrium precipitate. With higher elastic strain energy contribution, while the critical nucleus maintains the cubic symmetry, the equilibrium precipitate becomes plate-like with only the twofold symmetry.

As we further increase the elastic energy contribution, for example, $\beta = 3$ in Fig. 6, both the critical nucleus and the equilibrium precipitate exhibit plate-shaped particles. We also observe the increases in both the critical nucleus size and the nucleation energy barrier with increasing elastic energy contributions.

From the above numerical examples for modeling the cubic to tetragonal phase transformation in a conserved field, similar as the cubic to cubic transformation [23], we can see that the elastic energy plays an important role to determine the morphologies of both the critical nucleus and the equilibrium solution. For the same β, the influence of elastic energy on the critical nucleus and equilibrium solution may be different. Depending on the competition between the elastic energy

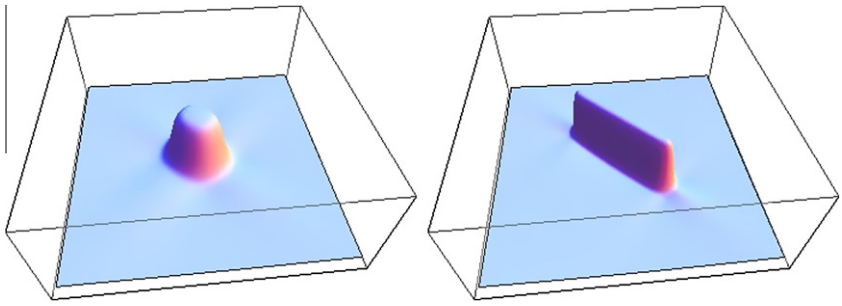

Fig. 6. Critical nucleus and equilibrium precipitate for $\beta = 3$.

and interfacial energy, the shapes of the critical nuclei may either keeping the cubic symmetry or changing to a twofold symmetry. Furthermore, choosing the different types of the stress-free strain can result in different orientations of the critical nucleus and the equilibrium solution.

3.2. Two orientation variants in a non-conserved field

In order to extend our method to more general cases, we next consider a case with two long-range order parameters $\eta_1 = \eta_1(x)$ and $\eta_2 = \eta_2(x)$, with each of them characterizes the shape, size, and spatial distribution of one of the two orientation domains.

The total free energy contains non-local gradient terms, a bulk free energy, $f(\eta_1, \eta_2)$, and elastic energy, i.e.,

$$E_{total} = \int_{\Omega} \left[\frac{1}{2}(\alpha_1 |\nabla \eta_1(x)|^2 + \alpha_2 |\nabla \eta_2(x)|^2) + f(\eta_1(x), \eta_2(x)) \right] dx + \beta \cdot E_{elastic},$$

where α_1, α_2 are gradient energy coefficients.

The bulk free energy is usually approximated by a Landau-type polynomial expansion following the symmetry operations with respect to the parent phase. Here we choose an expansion with terms up to sixth order, so it is written as

$$f(\eta_1, \eta_2) = \frac{a\lambda}{2}(\eta_1^2 + \eta_2^2) - \frac{b\lambda}{4}(\eta_1^4 + \eta_2^4) + \frac{c\lambda}{6}(\eta_1^2 + \eta_2^2)^3.$$

To choose some suitable parameters, a couple of conditions should be satisfied:

$$f_x(\pm 1, 0) = 0, \quad f_y(0, \pm 1) = 0,$$
$$f(\pm 1, 0) < f(0, 0) = 0.$$

So it turns out that

$$a - b + c = 0; \quad \frac{a}{2} - \frac{b}{4} + \frac{c}{6} < 0.$$

One example is shown in Fig. 7, where we take $a = 2$, $b = 19$, $c = 17$ and $\lambda = 1$. It is easy to see that the initial cubic phase is located at $(\eta_1, \eta_2) = (0, 0)$ and the final tetragonal phase takes place at $(\eta_1, \eta_2) = (\pm 1, 0)$ *or* $(0, \pm 1)$ which depends on different orientation domains.

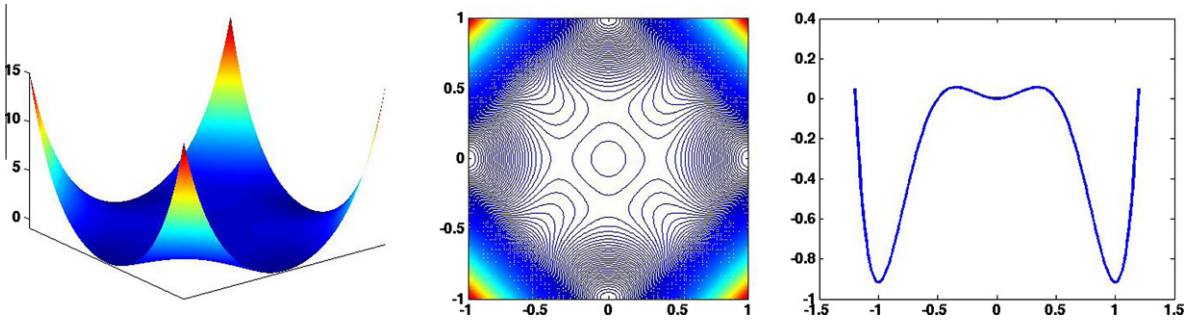

Fig. 7. Free energy surface, contour, free energy for one single domain.

In a two-dimensional analogue, the tetragonal phase forms two orientation variants in the cubic phase matrix. Without considering the dilatational components, one can choose the stress-free strains of two variants as

$$\epsilon^0(1) = \epsilon_0 \begin{pmatrix} 1 & 0 \\ 0 & -1 \end{pmatrix}; \quad \epsilon^0(2) = \epsilon_0 \begin{pmatrix} -1 & 0 \\ 0 & 1 \end{pmatrix}$$

where ϵ_0 is a constant.

Following Khachaturyan's theory [27], we can derive an explicit form of the elastic energy:

$$E_{elastic} = \frac{1}{2} \sum_{p,q=1}^{2} \overline{B}_{pq} \int \eta_p^2(x) \eta_q^2(x) dx - \frac{1}{2} \sum_{p,q=1}^{2} \int \frac{dk}{(2\pi)^2} B_{pq}(\mathbf{n}) \widetilde{(\eta_p^2)}(k) \widehat{(\eta_q^2)}(k), \tag{11}$$

where

$$\begin{aligned}
&\overline{B}_{11} = \overline{B}_{22} = 2\epsilon_0^2(c_{11} - c_{12}), \quad \overline{B}_{12} = \overline{B}_{21} = -\overline{B}_{11}, \\
&B_{11}(\mathbf{n}) = B_{22}(\mathbf{n}) = -\frac{\epsilon_0^2(c_{11} - c_{12})^2(c_{44} + 2(c_{11} + c_{12})n_1^2 n_2^2)}{c_{44} D(\mathbf{n})}, \\
&B_{12}(\mathbf{n}) = B_{21}(\mathbf{n}) = -B_{11}(\mathbf{n}), \\
&D(\mathbf{n}) = c_{11} + \xi(c_{11} + c_{12}) n_1^2 n_2^2, \quad \xi = \frac{c_{11} - c_{12} - 2c_{44}}{c_{44}}.
\end{aligned}$$

Once again as an illustration, the two-dimensional example of a cubic to tetragonal transformation is considered within the homogeneous modulus approximation in a non-conserved field. The computational set-up and the parameters used are as follows. The string is discretized by $m = 50$ points and the spatial simulation grid is maintained as 256×256. Numerical verification was conducted to ensure that there is enough resolution. We choose the coefficients of the bulk free energy $a = 2$, $b = 20$, $c = 18$ that gives the parameter λ which determines the energy difference between two well depths. Some other parameters are $\alpha_1 = \alpha_2 = 1.56 \times 10^{-4}$, $c_{11} = 250$, $\lambda = 0.15$, $c_{12} = 150$, $c_{44} = 100$, and $\epsilon_0 = 0.01$.

In Fig. 8, we compute the order parameter profiles for both critical nucleus (left) and equilibrium structure (right) at $\beta = 0.5$. It shows that the critical nucleus has a single-variant structure, nevertheless the equilibrium structure appears a two-variant polytwinned microstructure due to the long-range elastic interactions.

One interesting result is shown in Fig. 9. The order parameter profiles show that the critical nucleus has a two-variant twin shape, and the equilibrium structure displays a two-variant polytwinned microstructure which is identical with that in Fig. 8 because of the periodicity. It indicates that the highly spatially correlated polytwinned domain structure could be formed by the twin-shape critical nucleus. If we increase the elastic energy by taking $\beta = 1.5$ in Fig. 10, both the critical nucleus and the equilibrium solution keep the similar configurations as Fig. 9.

To offer a more intuitive observation, we plot the order parameter profiles along the diagonal direction in Fig. 11. For the comparison of the critical nuclei in Fig. 11 (left), it can be seen that the critical nucleus at $\beta = 1.5$ is larger than that at $\beta = 0.5$, and the maximum value of critical nucleus at $\beta = 1.5$ is also bigger than that at $\beta = 0.5$. For the different equilibrium solutions in Fig. 11 (right), it shows that the interface of the equilibrium one at $\beta = 1.5$ becomes more diffuse than that at $\beta = 0.5$. This is because when the elastic energy increases, coupling of two variants with more diffuse-interface reduces the per-volume elastic energy even at a cost of an increasing interfacial energy. Also, the order parameter value at the equilibrium phase at $\beta = 1.5$ is smaller than that at $\beta = 0.5$, which can be explained by the fact that the elastic interaction functions as the bulk energy. Moreover, we notice that the critical nucleation energy increases from 1.81×10^{-4} ($\beta = 0.5$) to 2.83×10^{-4} ($\beta = 1.5$), and the energy of the equilibrium precipitate increases from -0.0307 ($\beta = 0.5$) to -0.0074 ($\beta = 1.5$).

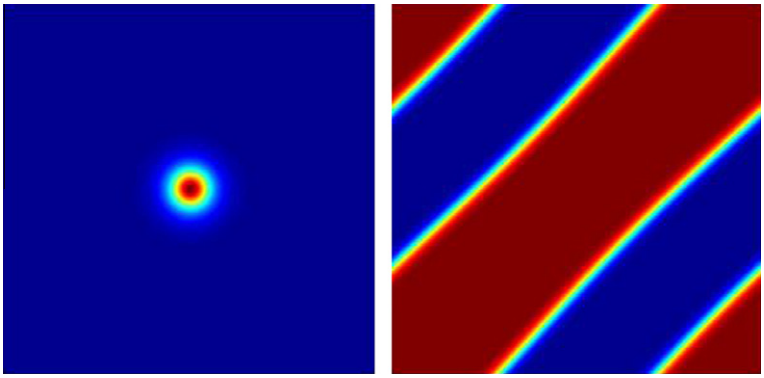

Fig. 8. Order parameter profiles of critical nucleus (left) and equilibrium particle (right).

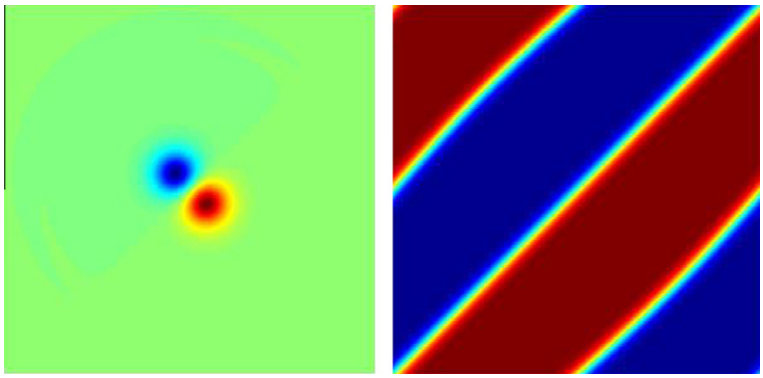

Fig. 9. Order parameter profiles of critical nucleus (left) and equilibrium particle (right) at $\beta = 0.5$.

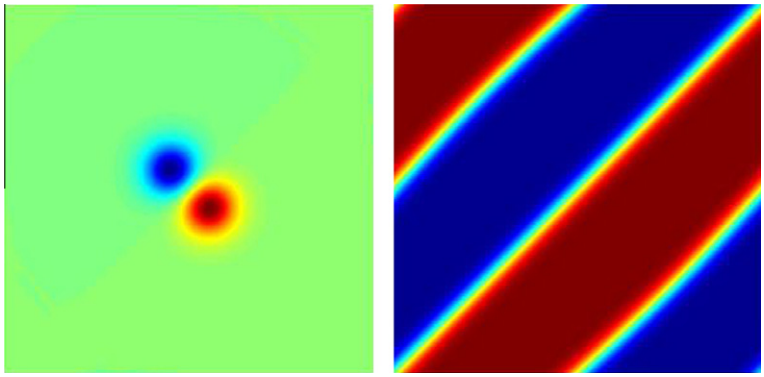

Fig. 10. Order parameter profiles of critical nucleus (left) and equilibrium particle (right) at $\beta = 1.5$.

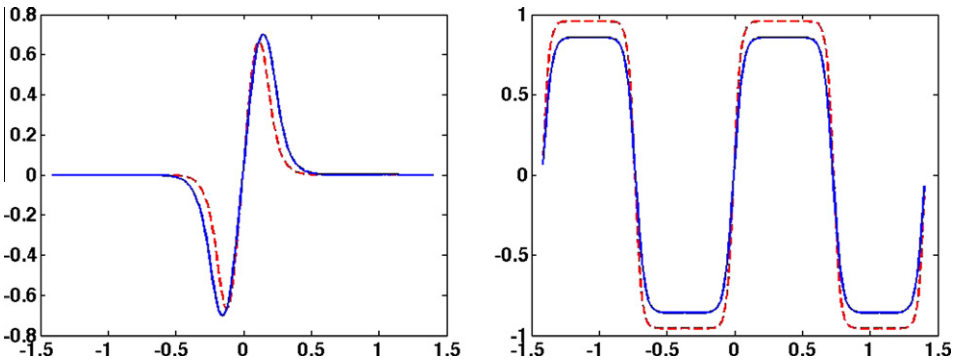

Fig. 11. Order parameter profiles of critical nucleus (left) and equilibrium particle (right) along the diagonal direction. Red dashed line: $\beta = 0.5$; blue solid line: $\beta = 1.5$. (For interpretation of the references in colour in this figure legend, the reader is referred to the web version of this article.)

The examples provided here serve to illustrate the effectiveness of the diffuse-interface model developed here to study the cubic to tetragonal nucleations. It is expected that more understanding of this important process can be obtained through further simulations, in particular for the case of the two-variant nucleation. The latter will be pursued in future works.

4. Summary

In this work, we extended our earlier studies to take advantage of the generality of the diffuse-interface approach in the study of nucleation in solid-state transformations. By combining the diffuse-interface model with the constrained string method, we were able to compute the morphologies of both critical nuclei and equilibrium microstructures for cubic to

tetragonal transformation without *a priori* shape assumptions. We conducted a series of preliminary numerical experiments that demonstrated the effectiveness of our new approach. Moreover, the limited experiments can already offer insights into the complicated nucleation process. For example, we find that choosing the different stress-free strains can lead to different orientations of the critical nuclei and the equilibrium twin structures in cubic to tetragonal transformation. It is also shown that the elastic energy contribution may lead to different symmetries in the morphologies of critical nucleus and equilibrium microstructure. In addition, for the nucleation of the two variants, an interesting observation is that the polytwinned domain structure can be formed by the twin-shape critical nucleus. We will utilize the models and algorithms developed here to carry out more systematic simulations in the future in order to gather more quantitative information on the cubic to tetragonal nucleations.

References

[1] Y. Wang, L.Q. Chen, A.G. Khachaturyan, Kinetics of strain-induced morphological transformation in cubic alloys with a miscibility gap, Acta Mater. 41 (1993) 279–296.
[2] H.J. Jou, P.H. Leo, J.S. Lowengrub, Microstructural evolution in inhomogeneous elastic media, J. Comput. Phys. 131 (1997) 109–148.
[3] J.K. Lee, Morphology of coherent precipitates via a discrete atom method, Mater. Sci. Eng. A 238 (1997) 1–12.
[4] R. Mueller, D. Gross, 3D simulation of equilibrium morphologies of precipitates, Comput. Mater. Sci. 11 (1998) 35–44.
[5] G. Henkelman, H. Jonsson, Improved tangent estimate in the nudged elastic band method for finding minimum energy paths and saddle points, J. Chem. Phys. 113 (2000) 9978.
[6] G. Henkelman, B. Uberuaga, H. Jónsson, A climbing image nudged elastic band method for finding saddle points and minimum energy paths, J. Chem. Phys. 113 (2000) 9901–9904.
[7] W. E, W. Ren, E. Vanden-Eijnden, String method for the study of rare events, Phys. Rev. B 66 (2002) 052301.
[8] W. E, W. Ren, E. Vanden-Eijnden, Simplified and improved string method for computing the minimum energy paths in barrier-crossing events, J. Chem. Phys. 126 (2007) 164103.
[9] C. Qiu, T.Z. Qian, W. Ren, Application of the string method to the study of critical nuclei in capillary condensation, J. Chem. Phys. 129 (2008) 154711.
[10] M. Venturoli, E. Vanden-Eijnden, G. Ciccotti, Kinetics of phase transitions in two dimensional Ising models studied with the string method, J. Math. Chem. 45 (2009) 188–222.
[11] L. Lin, X. Cheng, W. E, A.-C. Shi, P. Zhang, A numerical method for the study of nucleation of ordered phases, J. Comput. Phys. 229 (2010) 1797–1809.
[12] P. Rabinowitz, Minimax Methods in Critical Point Theory with Applications to Differential Equations, AMS, Providence, 1986.
[13] R. Glowinski, P.L. Tallec, Augmented Lagrangian and Operator-Splitting Methods in Nonlinear Mechanics, SIAM, 1989. AMS, Providence, 1986.
[14] M.E. Thompson, P.W. Voorhees, Equilibrium particle morphologies in elastically stressed coherent solids, Acta Mater. 47 (1999) 983–996.
[15] C. Wolverton, First-principles prediction of equilibrium precipitate shapes in Al–Cu alloys, Philos. Mag. Lett. 79 (1999) 683–690.
[16] A. Roy, J.M. Rickman, J.D. Gunton, K.R. Elder, Simulation study of nucleation in a phase-field model with nonlocal interactions, Phys. Rev. E 57 (1998) 2610–2617.
[17] C. Shen, J.P. Simmons, Y. Wang, Effect of elastic interaction on nucleation: I. Calculation of the strain energy of nucleus formation in an elastically anisotropic crystal of arbitrary microstructure, Acta Mater. 54 (2006) 5617–5630.
[18] C. Shen, J. Li, Y. Wang, Finding critical nucleus in solid-state transformations, Metall. Mater. Trans. A 39A (2008) 976–983.
[19] Q. Du, L. Zhang, A constrained string method and its numerical analysis, Commun. Math. Sci. 7 (2009) 1039–1051.
[20] L. Zhang, L.Q. Chen, Q. Du, Morphology of critical nuclei in solid state phase transformations, Phys. Rev. Lett. 98 (2007) 265703.
[21] L. Zhang, L.Q. Chen, Q. Du, Diffuse-interface description of strain-dominated morphology of critical nuclei in phase transformations, Acta Mater. 56 (2008) 3568–3576.
[22] L. Zhang, L.Q. Chen, Q. Du, Mathematical and numerical aspects of phase-field approach to critical morphology in solids, J. Sci. Comput. 37 (2008) 89–102.
[23] L. Zhang, L.Q. Chen, Q. Du, Simultaneous prediction of morphologies of a critical nucleus and an equilibrium precipitate in solids, Commun. Comput. Phys. 7 (2010) 674–682.
[24] L.Q. Chen, J. Shen, Applications of semi-implicit Fourier-spectral method to phase field equations, Comput. Phys. Commun. 108 (1988) 147–158.
[25] Q. Du, J. Zhang, Numerical studies of discrete approximations to the Allen–Cahn equation in the sharp interface limit, SIAM J. Sci. Comput. 31 (2009) 3042–3063.
[26] J. Cahn, J. Hilliard, Free energy of a nonuniform system. III: Nucleation in a two-component incompressible fluid, J. Chem. Phys. 31 (1959) 688–699.
[27] A.G. Khachaturyan, Theory of Structural Transformations in Solids, Wiley, New York, 1983.
[28] T.W. Heo, L. Zhang, Q. Du, L.Q. Chen, Incorporating diffuse-interface nuclei in phase-field simulations, Scripta Mater. 63 (2010) 8–11.